Investigation of the Structure of Oxidized *Pseudomonas aeruginosa* Cytochrome *c*-551 by NMR: Comparison of Observed Paramagnetic Shifts and Calculated Pseudocontact Shifts†

Russell Timkovich* and Mengli Cai

Department of Chemistry, University of Alabama, Tuscaloosa, Alabama 35487-0336

Received June 29, 1993®

ABSTRACT: Extensive main-chain and side-chain assignments are reported for the ^{1}H NMR spectrum of ferricytochrome *c*-551 from *Pseudomonas aeruginosa* at 323 K and pH 5.2. These were obtained by sequential assignments of two-dimensional scalar and dipolar correlation spectra. The low-spin ($S = {}^1/_2$) ferric iron in the oxidized state gives rise to extensive contact and pseudocontact shifts for resonances in the ferricytochrome. Total redox-state-dependent shifts were computed by comparison to the previously assigned ferrocytochrome *c*-551. A set of 179 firmly assigned protons was selected that were expected to experience only pseudocontact shift contributions in the oxidized form. The pseudocontact shifts were calculated for the set by a standard model [Williams, G., Clayden, N. J., Moore, G. R., & Williams, R. J. P. (1985) *J. Mol. Biol. 183*, 447–460] using the atomic coordinates from the X-ray crystallographic determination of the oxidized form [Matsuura, Y., Takano, T., & Dickerson, R. E. (1982) *J. Mol. Biol. 156*, 389–409], and effective anisotropy and geometric factors were adjusted to minimize the sum of the squared differences between observed redox-state shifts and calculated pseudocontact shift contributions. The root-mean-squared deviation with the optimized parameters was 0.12 ppm. The optimized model was then used to calculate pseudocontact shifts for other assigned protons outside the basic set. The overall agreement and the lack of any systematic discrepancies provide evidence that there are no major structural differences among the solution and crystal conformations of the oxidized and reduced forms, within the inherent resolution of this computational approach. The computation proved to be a powerful tool for the stereospecific assignment of 70 additional spin systems in cyt *c*-551. The optimized anisotropy showed principal axes aligned approximately along the directions of Fe–pyrrole nitrogen and Fe–ligand vectors.

Cytochrome *c*-551 (cyt *c*-551[1]) functions in an electron-transport chain of *Pseudomonas* in a manner analogous to that of cytochrome c in mitochondria. With ca. 82 amino acids it is approximately 20% smaller than cyt *c* and represents a minimum size protein capable of the same function. For all cytochromes, a central question has been what, if any, are the structural differences between the reduced and oxidized forms of the protein. Oxidized *P. aeruginosa* cyt *c*-551 was crystallized and an X-ray structure determined (Matsuura et al., 1982). The oxidized crystals were then reduced *in situ* by soaking them in sodium ascorbate. Difference electron density maps were calculated to investigate any structural changes. Reduction of the crystals was performed in part because of expediency. There were precedents that if one first reduced a cytochrome in solution and then attempted to crystallize it, a different space group with different packing could be, and was even likely to be, obtained (Takano et al., 1973, 1977; Swanson et al., 1977; Mandel et al., 1977; Takano & Dickerson, 1982a,b). This necessarily meant that the phase problem of crystallography would have to be solved anew, tantamount to starting over. The reduction of crystals raises the issue of whether the lattice forces have constrained the protein to a conformation that it would not normally take if free in solution.

Williams et al. (1985) demonstrated for horse cyt *c* that the paramagnetism of the iron in the oxidized form led to pseudocontact proton chemical shifts in the NMR spectrum that could be accurately accounted for by a relatively simple dipolar model for the unpaired ferric electron spin. Feng et al. (1990) extended these studies using a larger set of assigned resonances available from complete two-dimensional studies on horse cyt *c*. Gao et al. (1991) investigated the C102T mutant of yeast iso-1-cyt *c* by a similar approach, as did Veitch et al. (1990) for microsomal cyt b_5. The general strategy was as follows. Proton chemical shifts were measured for the reduced diamagnetic form of the protein, δ_{red}, and for the oxidized paramagnetic form, δ_{ox}. Protons within a certain number of covalent bonds of the iron, in practice, the heme itself, the ligands, and the cysteine thioether residues could have a contact shift contribution to their final oxidized shift, and so where excluded from the analysis of pseudocontact contributions. The observed differences in oxidized and reduced chemical shifts for other resonances were ascribed to a pseudocontact shift, $\delta_{pc,obs} = \delta_{ox} - \delta_{red}$. This contribution could be calculated from

$$\delta_{pc,calc} = -[\beta^2 S(S+1)/9kTr^3][G_{ax}(3\cos^2\theta - 1) + 1.5G_{eq}(\sin^2\theta\cos 2\phi)] \quad (1)$$

where G_{ax} and G_{eq} are effective anisotropies for an axially symmetric dipolar field and r, ϕ, and θ are spherical polar coordinates with respect to the principal axes.

The pseudocontact shift is a scalar field and depends upon the orientation of the principal axes within the molecule and the vector position of the proton within this field. The

† Financial support was provided in part by Grant GM43292 from the National Institutes of Health.

* Author to whom correspondence should be addressed.

® Abstract published in *Advance ACS Abstracts,* October 15, 1993.

[1] Abbreviations: cyt, cytochrome; NOE, nuclear Overhauser enhancement.

0006-2960/93/0432-11516$04.00/0

orientation and magnitude can be estimated initially from EPR measurements. To calculate the position, atomic coordinates from X-ray crystallographic determinations were required. All previous workers discovered that significant improvements could be made between $\delta_{pc,obs}$ and $\delta_{pc,calc}$ by slight adjustments in the orientation and magnitude of the anisotropies. Selections were made of a basis set of resonances, and G_{ax}, G_{eq}, and three Eulerian angles of orientation were optimized to produce the best fit between observed and calculated values for the basis set. Then, all assigned resonances were calculated and screened (using slightly different criteria) for significant differences between observed and calculated values. In this manner, it was possible to pinpoint regions where the final NMR chemical shift suggested that there were redox-related conformational differences. Although all studies agreed that the global folding in the two forms was constant, differences were found and the original reports should be consulted for further detailed discussion on the specific proteins.

Extensive resonance assignments are now available for the diamagnetic form of *P. aeruginosa* cyt *c*-551 (Chau et al., 1990; Detlefsen et al., 1990; Cai & Timkovich, 1991), as well as the crystal coordinates for the oxidized form (Matsuura et al., 1982). Herein is reported, for the first time, extensive main-chain and side-chain assignments for oxidized *P. aeruginosa c*-551 and the results of a comparison of predicted and observed pseudocontact shifts.

EXPERIMENTAL PROCEDURES

cyt *c*-551 was isolated as described previously (Chau et al., 1990). NMR spectroscopic methods and general conditions have been described (Cai et al., 1992). Oxidized samples typically contained 2–10 mg of analytical grade potassium ferricyanide from Mallinckrodt. Cobalt(III) phenanthroline was synthesized as described previously (Baker et al., 1959). The chemical shifts of resonances were referenced nominally against 3-(trimethylsilyl)propionic-d_4 acid sodium salt, but residual water was used as the actual internal reference and assigned a shift value of 4.48 ppm at 323 K and pH 5.2. Resonances for the reduced form have been assigned (Chau et al., 1990; Detlefsen et al., 1990), but since some of these are very pH-sensitive (Cai & Timkovich, 1991), a new data set was measured for the reduced protein at the same temperature and pH as the master oxidized data set for accurate computation of $\delta_{pc,obs}$.

A computer program to optimize the Euler angles of orientation, G_{ax}, and G_{eq} and then calculate $\delta_{pc,calc}$ was kindly donated by Dr. Gary Pielak of the University of North Carolina. The overall goodness of fit of the calculation is benchmarked by the root-mean-squared pseudocontact shift, defined by

$$\langle\delta_{pc}\rangle = \{[\sum(\delta_{pc,obs} - \delta_{pc,calc})^2]/n\}^{1/2} \quad (2)$$

where the summation is over the set of all resonances used in the calculation and n is the number in the set. Methyl protons are averaged. The program varies G_{ax} and G_{eq} from eq 1 and three rotational angles, α, β, and γ [defined in Williams et al. (1985)], that determine the rotation of the principal axes about an initial starting orientation, so as to minimize $\langle\delta_{pc}\rangle$. Heavy atom coordinates from the crystal structure of oxidized *P. aeruginosa* cyt *c*-551 were obtained from the Brookhaven Protein Data Bank. Hydrogens were added in standard geometries by the software package XPLOR (Kuszewski et al., 1992).

$\delta_{pc,calc}$ given by eq 1 is a scalar field that has a gradient associated with it. The magnitude of the gradient is independent of choice of coordinate system, but it is conveniently calculated from the spherical polar coordinates by

$$|\nabla\delta_{pc,calc}| = \left[\left(\frac{\partial\delta_{pc,calc}}{\partial r}\right)^2 + \left(\frac{\partial\delta_{pc,calc}}{r\,\partial\theta}\right)^2 + \left(\frac{\partial\delta_{pc,calc}}{r\sin\theta\,\partial\phi}\right)^2\right]^{1/2} \quad (3)$$

This quantity was used to assess any differences between $\delta_{pc,obs}$ and $\delta_{pc,calc}$ in terms of estimating how large of a displacement would be required to bring these quantities into agreement.

RESULTS

The assignment of the oxidized spectrum of cyt *c*-551 posed some special problems. Although the reduced spectrum has been well assigned, the paramagnetism scrambles so many resonances that the oxidized spectrum must be treated *de novo*. Saturation transfer techniques have been used previously to correlate resonances in an oxidized cyt *c* with the corresponding spin in the reduced form (Feng et al., 1989). This is not possible for *c*-551. The rate of electron self-exchange is orders of magnitude faster in *c*-551 than in cyt *c*, and this means that mixtures of the redox states lead to severe line broadening. Even a small fraction of reduced protein in the presence of the oxidized protein leads to the loss of spectral signal-to-noise [see Figure 1 of Timkovich et al. (1988) and Figure 2 of Keller and Wuthrich (1976)]. This is also the reason why an external oxidant, ferricyanide, was typically added to the NMR samples. It is known that pure ferricytochromes *c* in only phosphate buffer undergo an apparent "autoreduction" that is actually light-driven (Yu et al., 1975). The photoreduction mechanism is radical-based and has been studied in detail for model ferric porphyrins, where it was found that the net reducing equivalents could be provided by amines or even hydroxyl compounds (Del Gaudio & La Mar, 1978; Bartocci et al., 1980). cyt *c*-551 seems to be especially susceptible to this photoreduction, so that even though it is purified with the final steps in the oxidized state, upon simple handling and storage it begins to photoreduce. Rather than employ elaborate precautions to work with strict exclusion of light, it is simpler to add a small amount of an oxidant. Control experiments were performed in which the concentration of ferricyanide was varied and even replaced with a cationic oxidant, cobalt(III) phenanthroline, without discernible changes in the observed oxidized chemical shifts.

Even in a fully oxidized sample, the broadness of some resonances caused difficulties. Relaxation during the mixing time of NOESY spectra or during the spin lock time of HOHAHA spectra caused some expected or sought cross peaks not to be observed. COSY-type spectra do not have these time periods in the sequence, but the inherent dispersive line shapes also made already broad resonances difficult to discern above noise. The net impact was that fewer resonances could be assigned in the oxidized form than had been assigned in the reduced form. His 16 ring protons and Pro 60 and Pro 62 resonances were notable examples that could not be assigned.

The assignment process began with the well-resolved heme methyl resonances which appear to high frequency because of large contact shifts. These had been firmly assigned by previous one-dimensional studies (Keller & Wuthrich, 1978; Senn et al., 1980), and the final pattern of NOESY cross peaks involving these was only consistent with the original assignments. NOESY cross peaks identified meso and propionate resonances which were then confirmed by additional

NOEs and scalar correlations. A small number of landmark side chains was also identified on the basis of their spin system types and their proximity to the heme. These later proved to be valuable markers for the sequential assignment process. Residues distant from the heme (N-terminal residues 1–6, C-terminal residues 77–82, and residues 33–41) experienced only small pseudocontact shifts, and these could be identified by comparisons to reduced-form two-dimensional spectra. Thereafter, the remaining residues were assigned by a sequential strategy in which characteristic spin subsystems were linked by means of interresidue NOEs. The main NOEs were essentially the same as those found for reduced *c*-551 and are listed in Table III of Chau et al. (1990).

Assignments are listed in Table I. The 13-propionate resonances at 11.2 and 12.6 ppm were previously assigned to the 17-propionate (Leitch et al., 1984) on the basis of a one-dimensional difference NOE experiment that showed these resonances to be close to protons of Trp 56. However, both propionates satisfy this condition, and the present assignment is only consistent with strong two-dimensional NOESY cross peaks involving the 12^1 methyl. Tentative assignments had been proposed for resonances around 0 ppm only on the basis of analogy to oxidized horse cyt *c* (Timkovich, 1991). These were incorrect, and the peaks are now assigned to meso 20 and Ile 48 side-chain protons.

The initially assumed orientation of the principal axes was consistent with the results of earlier EPR studes (Chao et al., 1979), with the *x* and *y* principal axes located along orthogonal iron–pyrrole nitrogen directions and the *z* axis perpendicular to the heme plane, as shown in Figure 1 of Feng et al. (1990) with the spherical coordinates also defined therein. It should be noted that because of the periodicity of the trigonometric functions in eq 1, rotations of the coordinate system about the *z* axis by multiples of $\pi/2$ radians, inversion of the *z* axis, or interchange of the *x* and *y* axes do not change the computed $\delta_{pc,calc}$, although the sign of G_{eq} may change. A qualitative inspection of the oxidized-form chemical shifts confirmed that the pseudocontact scalar field has axial symmetry. This roughly means that protons located near to the *z* axis perpendicular to the heme plane have shifts to higher frequency in the oxidized form ($\delta_{pc,obs} > 0$), while protons near to the mean heme plane have shifts to lower frequency. The magnitude falls rapidly as the distance from the iron increases.

For quantitative calculations, a basis set was selected of 179 firmly assigned resonances spread along the entire polypeptide chain (specified in Table I). Included were main-chain amide, α, and side-chain protons where there was no question of stereospecificity (such as the β-protons of alanine, valine, and isoleucine). Heme, ligand, and thioether cysteine protons were excluded since they were expected to experience contact shift contributions.

The magnitudes of the **g** tensor components ($g_z = 3.24$, $g_x = 2.06$, $g_y = 1.48$) have been measured for oxidized *c*-551 at liquid helium temperatures (Chao et al., 1979; Gadsby & Thomson, 1990). Initial estimates of G_{ax} and G_{eq} have been made by previous workers (Feng et al., 1990; Gao et al., 1991) based upon the following relations:

$$G_{ax} = g_z^2 - 0.5(g_x^2 + g_y^2) \quad (4a)$$

$$G_{eq} = g_x^2 - g_y^2 \quad (4b)$$

The room-temperature pseudocontact shifts are more precisely related to the magnetic susceptibilities at the corresponding temperature (Horrocks & Greenberg, 1973). These have been calculated from the low-temperature *g* values by considering first- and second-order Zeeman terms, electronic energy levels, and spin-obital coupling constants (Horrocks & Greenberg, 1973; Williams et al., 1985; Emerson & LaMar, 1990; Rajarathnam et al., 1992, 1993; Turner & Williams, 1993). However, even in these cases, when extensive NMR pseudocontact shifts have been calculated, it has been found that significant improvement in the fit occurs with further optimization of the magnitudes of the susceptibilities (Rajaratham et al., 1992, 1993; Turner & Williams, 1993). There does not appear to us to be a consensus method for the calculation of the room-temperature susceptibilities [for a discussion, see Turner and Williams (1993)], and since they are likely to require refinement anyway, the simplest approach was taken and eq 4 was used to estimate starting values of $G_{ax} = 7.28$ and $G_{eq} = 2.05$. In previous cases, the final best magnitudes were found to be close to the EPR-derived ones, with an orientation close to *x* and *y* being near Fe-N directions and *z* within 10° of the heme normal. In the *c*-551 calculation, it was clear that the initial parameters gave the proper sign to $\delta_{pc,calc}$, but that the absolute magnitude was consistently too high. The value of $\langle\delta_{pc}\rangle$ was 0.59 ppm. When G_{ax} and G_{eq} were fixed and the angles of orientation optimized, some improvement occurred, but the lowest value of $\langle\delta_{pc}\rangle$ was still 0.47 ppm. When G_{ax} and G_{eq} were allowed to vary, dramatic improvement in the fit occurred. With the final optimized values $G_{ax} = 4.35$, $G_{eq} = 1.40$, $\alpha = 54°$, $\beta = -5°$, and $\gamma = -28°$, $\langle\delta_{pc}\rangle$ was 0.12 ppm. These results can be contrasted with previous calculations on other cytochromes. Similar to the previous studies, the value of β was within 10° of the heme normal and the sum $\alpha + \gamma$ was close to 360°, indicating near coincidence of *x* and *y* with Fe–N directions. For horse cyt *c* (Feng et al. (1990), the EPR-derived values were $G_{ax} = 6.05$ and $G_{eq} = 3.50$, while after optimization $G_{ax} = 4.92$ and $|G_{eq}| = 1.79$, giving $\langle\delta_{pc}\rangle = 0.13$ ppm for a basis set of 80 α-protons. For the C102T variant of yeast iso-1-cyt *c* (Gao et al., 1991), the EPR-derived values were assumed to be the same as for horse cyt *c*, while after optimization $G_{ax} = 4.58$, $|G_{eq}| = 2.31$, giving $\langle\delta_{pc}\rangle = 0.21$ for 342 amide, α-, and β-protons. For cyt b_5 (Veitch et al., 1990), the EPR-derived values were $G_{ax} = 5.67$ and $|G_{eq}| = 2.93$, while after optimization $G_{ax} = 5.25$ and $|G_{eq}| = 2.31$, giving $\langle\delta_{pc}\rangle = 0.14$ ppm. The *c*-551 calculation is therefore very comparable to previous studies, except for the larger changes in G_{ax} and G_{eq} from the initial starting values.

After optimization, an examination of the strong agreement between $\delta_{pc,obs}$ and $\delta_{pc,calc}$ for resonances distributed throughout the protein indicated that the NMR data were very consistent with the coordinates from the oxidized crystal structure. Calculation of $\delta_{pc,calc}$ for all protons then provided a powerful tool for the stereospecific assignment of such spin systems as the β-methylene protons of aspartate residues, etc. The atomic coordinates of the chiral protein differentiate between the pair. Initially, there are two resonances (two chemical shifts) for the pair in the oxidized form and another pair for the reduced. Without stereospecific assignment, there are thus two ways to form $\delta_{pc,obs}$. If the coordinates of the protons predict sufficiently different values for $\delta_{pc,calc}$, then it is possible to find a unique combination for $\delta_{pc,obs}$ that in turn will lead to stereospecific assignments in both oxidation states. An example will illustrate. The γ-methyl protons of Val 13 were found in the oxidized form at 0.80 and 0.99 ppm, while in the reduced form they were at 0.64 and 0.85 ppm. Based upon the atomic coordinates from the crystal structure, $\delta_{pc,calc}$ was –0.06 for HG1 and +0.25 for HG2. Clearly the best fit is to assign HG1 as 0.80 ppm in the oxidized form and 0.85 ppm

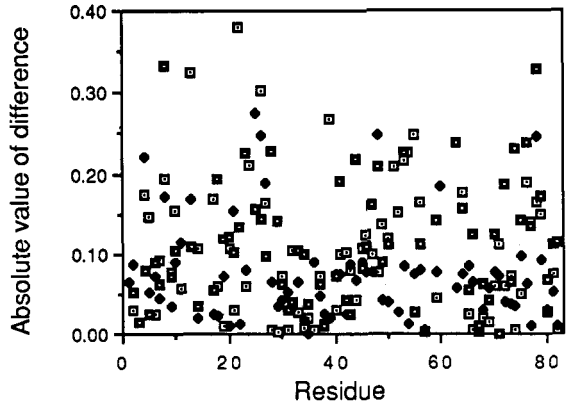

FIGURE 1: Plot of the absolute value of the difference, $|\delta_{pc,obs} - \delta_{pc,calc}|$, between observed paramagnetic shifts and calculated pseudocontact shift contributions for oxidixed *P. aeruginosa* cyt *c*-551. Data are plotted for assigned amide (□) and α (◆) protons. For other resonances associated with a given residue, the maximum difference for the spin subsystem was plotted (■) as discussed in the text.

in the reduced form. In this fashion, 70 stereospecific assignments were achieved for both forms of *c*-551. For cases where additional scalar and NOE data were available, the pseudocontact shift-based assignments were consistent with those from other traditional techniques for making stereospecific discriminations (Cai et al., 1992). This approach is quite powerful, but not universal. It fails when $\delta_{pc,calc}$ is not sufficiently different within the pair or when one cannot discriminate between the alternative ways of forming $\delta_{pc,obs}$. These instances become more common as the distance from the paramagnetic center increases.

$\delta_{pc,calc}$'s were computed for resonances close to the iron that had been excluded from the basis set because of the possibility of major contact shift contributions. Heme protons, thioether bridge methyl and methine protons, and the γ- and ϵ-protons of Met 61 had observed shifts far in excess of $\delta_{pc,calc}$ because of major contact contributions. The imidazole protons of His 16 have not been assigned in the oxidized form. As shown in Table I, the amide and α-protons of the ligand and bridge residues have good agreement between observed and calculated values, except for Cys 15 HA. Some of the β-protons have good agreement while others do not, suggesting that the contact shift contribution has diminished for this number of bonds from the iron, but not in a simply predicted fashion.

Figure 1 displays $|\delta_{pc,obs} - \delta_{pc,calc}|$ for the basis set used in optimization, the set of stereospecifically assigned protons, and others which could be reasonably matched in both redox forms. The latter set included many pairs for which stereospecific assignments could not be firmly made. In such cases, the resonances were matched across the redox states so as to maximize $|\delta_{pc,obs} - \delta_{pc,calc}|$. Heme, ligand, and bridge resonances were excluded, along with a special set of problem resonances that will be discussed separately. The significance of the figure is that there is no discernible systematic difference between observed and calculated values over the whole protein. If one takes $\langle\delta_{pc}\rangle$ as a measure of the standard deviation σ for a normal distribution, then it is seen that most discrepancies are within 2σ, with only a few as bad as 3σ.

Protons associated with several residues had large values for $|\delta_{pc,obs} - \delta_{pc,calc}|$. All benzoid side chains undergo rapid motion about the C1–C4 axis in cyt *c*-551 (Chau et al., 1990; Cai et al., 1992). This it makes it ambiguous to assign the ring protons to atomic coordinates from the crystal structure. The use of simple average coordinates in this case does not seem justified, because the average would be within the carbon ring at a position where the proton could never experience the scalar pseudocontact field. Since it is not known whether the ring motion is strictly 180° flipping or a motion with some wobbling associated, more sophisticated coordinate averaging is not possible. For Phe 7 and Tyr 27, the pseudocontact field changes very rapidly in the vicinity of the ring, and whatever averaging takes place leads to a large discrepancy between $\delta_{pc,obs}$ and $\delta_{pc,calc}$. On the other hand, the field is fairly constant near Phe 34, and this gives an apparent and probably false impression of agreement.

Protons associated with 10 residues had large differences that were difficult to interpret. These included Val 13 HB, Gly 24 HA, Pro 25 HD, Arg 47 HD, Ile 48 HD, Gly 51 HA, Ser 52 HB, Pro 58 HA, HB, and HD, Ile 59 HG2, and Trp 77 HH protons. The magnitude of the gradient of the pseudocontact shift contribution was calculated at the atomic positions from the crystal coordinates. The magnitude of the gradient is an estimate of the effect for an infinitesimal displacement in the direction that would produce the maximum change in $\delta_{pc,calc}$. The ratio of $|\delta_{pc,obs} - \delta_{pc,calc}|$ to the magnitude of the gradient is therefore an estimate of how far the proton would have to be displaced in order to bring the discrepancy in line. It is only an estimate because the gradient is a continuously variable vector quantity that changes as the position of the proton changes. However, it does provide an insight into how serious a given discrepancy may be. Table I shows that modest movements of Gly 24 HA, Pro 25 HD, Arg 47 HD, Ile 48 HD, Gly 51 HA, Ser 52 HB, and Trp 77 HH protons could appreciably reduce the discrepancies and bring them to within 3 times $\langle\delta_{pc}\rangle$ as a measure of 3σ. Val 13, Pro 58, or Ile 59 would have to experience major displacements to bring some of their resonances into agreement. It seems unlikely that there could be such a global structure change, because the neighboring amide, α-, and γ-protons all show good agreement with calculation. Veitch et al. (1990) also encountered a small number of major discrepancies for a few protons in cyt b_5 (Val 45 and Gly 42) that could not be accounted for by a peptide segment movement. They suggested that increased mobility about an average position that matched the crystal coordinates might account for the discrepancy.

DISCUSSION

The most basic conclusion from the computation of $\delta_{pc,calc}$ is that there are no major structural differences among the crystal and solution conformations of oxidized and reduced *P. aeruginosa c*-551, within the total limitations of all facets of the technique. These limitations, which can be said to give rise to an effective resolution for discerning structural change, include the chemical shift measurements, the accuracy of the crystal atomic coordinates, whether crystal forces have produced changes from either redox-state solution structure, and any limitations in the use of eq 1. Different groups have analyzed discrepancies between $\delta_{pc,obs}$ and $\delta_{pc,calc}$ in different manners, and the present study has attempted to draw upon only the main elements of past work. The comparisons made in Figure 1 accentuate only the magnitude of any discrepancy and in this regard are more similar to the analyses of the "Oxford" school of thought (Williams et al., 1985; Gao et al., 1991; Turner & Williams, 1993). Feng et al. (1990) used a more elaborate "screen" for structural change in ferricytochrome *c* that was based not only upon discrepancies calculated for five different parameter sets but also upon a consideration of possible crystal coordinate errors, a maximum pseudocontact shift gradient, and whether a critical displacement in proton position could bring calculation and observation into agree-

Table I: Assignments for Oxidized and Reduced *P. aeruginosa* cyt *c*-551 and the Results of the Pseudocontact Shift Computations[a]

sequence	residue	atom	use	oxidized	reduced	obs	calc	gradient	sequence	residue	atom	use	oxidized	reduced	obs	calc	gradient
1	Glu	HA	B	4.00	4.01	−0.01	−0.08	0.01	18	Ile	HG11	S	1.80	1.25	0.55	0.38	0.09
2	Asp	HN	B	8.96	9.02	−0.06	−0.09	0.02	18	Ile	HG12	S	1.28	0.80	0.48	0.29	0.08
2	Asp	HA	B	4.77	4.79	−0.02	−0.11	0.02	18	Ile	HG23	B	1.05	0.59	0.46	0.48	0.17
2	Asp	HB1	T	2.73	2.76	−0.03	−0.08	0.02	18	Ile	HD3	B	0.97	0.55	0.42	0.27	0.07
2	Asp	HB2	T	2.56	2.59	−0.03	−0.07	0.01	19	Asp	HN	B	8.54	7.98	0.56	0.57	0.13
3	Pro	HD1	T	3.52	3.65	−0.13	−0.12	0.02	19	Asp	HA	B	5.00	4.50	0.50	0.43	0.09
3	Pro	HD2	T	3.73	3.90	−0.17	−0.16	0.03	19	Asp	HB1	S	2.75	2.47	0.28	0.33	0.06
4	Glu	HN	B	8.14	8.08	0.06	−0.11	0.03	19	Asp	HB2	S	2.96	2.47	0.49	0.37	0.07
4	Glu	HA	B	3.41	3.27	0.14	−0.08	0.05	20	Thr	HN	B	7.24	6.46	0.78	0.67	0.16
4	Glu	HB1	T	1.92	1.95	−0.03	−0.02	0.03	20	Thr	HA	B	4.87	4.33	0.54	0.53	0.12
4	Glu	HB2	T	2.23	2.36	−0.13	−0.05	0.02	20	Thr	HB	B	4.21	3.67	0.54	0.45	0.10
5	Val	HN	B	7.08	7.03	0.05	−0.10	0.03	20	Thr	HG3	B	1.36	0.87	0.49	0.37	0.07
5	Val	HA	B	3.65	3.67	−0.02	−0.07	0.02	21	Lys	HN	B	8.88	8.26	0.62	0.59	0.15
5	Val	HB	B	2.11	2.18	−0.07	−0.09	0.02	21	Lys	HA	B	4.64	3.53	1.11	1.26	0.41
5	Val	HG13	T	0.83	0.92	−0.09	−0.07	0.01	21	Lys	HB1	S	2.15	1.68	0.47	0.53	0.16
5	Val	HG23	T	0.95	0.98	−0.03	−0.05	0.01	21	Lys	HB2	S	2.25	1.63	0.62	0.72	0.24
6	Leu	HN	B	7.39	7.52	−0.13	−0.15	0.04	21	Lys	HG1	T	1.77	1.07	0.70	1.02	0.43
6	Leu	HA	B	3.93	4.04	−0.11	−0.18	0.04	22	Met	HN	B	8.36	7.26	1.10	1.48	0.54
6	Leu	HB1	S	1.68	2.00	−0.32	−0.31	0.09	22	Met	HA	B	4.91	4.36	0.55	0.54	0.18
6	Leu	HB2	S	1.06	1.30	−0.24	−0.27	0.07	22	Met	HB1	S	2.46	1.91	0.55	0.55	0.23
6	Leu	HG	B	1.47	1.72	−0.25	−0.16	0.04	22	Met	HB2	S	2.63	1.24	1.39	1.25	0.51
6	Leu	HD13	S	0.72	0.93	−0.21	−0.22	0.05	22	Met	HG1	T	2.77	1.52	1.25	1.04	0.32
6	Leu	HD23	S	0.77	0.91	−0.14	−0.15	0.04	23	Val	HN	B	7.59	6.87	0.72	0.66	0.45
7	Phe	HN	B	7.97	8.28	−0.31	−0.22	0.08	23	Val	HA	B	3.81	3.91	−0.10	−0.18	0.27
7	Phe	HA	B	3.93	4.28	−0.35	−0.39	0.20	23	Val	HB	B	1.13	1.83	−0.70	−0.93	0.78
7	Phe	HB1	S	2.89	2.92	−0.03	−0.09	0.10	23	Val	HG13	S	−0.06	1.54	−1.60	−1.59	0.70
7	Phe	HB2	S	2.82	3.00	−0.18	−0.21	0.16	23	Val	HG23	B	0.63	1.12	−0.49	−0.47	0.26
7	Phe	HD1	T	7.14	7.23	−0.09	0.08	0.11	24	Gly	HN	B	8.62	6.62	2.00	1.79	1.63
7	Phe	HD2	T	7.14	7.23	−0.09	−0.04	0.48	24	Gly	HA1	S	5.58	0.06	5.52	4.33	6.12
7	Phe	HE1	T	6.88	6.91	−0.03	0.30	0.14	24	Gly	HA2	S	5.58	3.68	1.90	0.38	1.67
7	Phe	HE2	T	6.88	6.91	−0.03	1.20	0.84	25	Pro	HA	T	5.20	3.57	1.63	1.35	0.69
7	Phe	HZ1	T	7.03	7.04	−0.01	0.76	0.34	25	Pro	HB1	T	1.51	0.97	0.54	0.65	0.56
8	Lys	HN	B	7.02	6.94	0.08	−0.11	0.06	25	Pro	HB2	T	1.73	0.52	1.21	1.05	0.75
8	Lys	HA	B	3.98	3.88	0.10	−0.07	0.08	25	Pro	HG1	T	0.44	0.32	0.12	0.02	1.11
8	Lys	HB1	T	1.87	1.84	0.03	−0.07	0.03	25	Pro	HG2	T	1.92	0.10	1.82	1.73	2.60
8	Lys	HB2	T	1.57	1.30	0.27	−0.06	0.04	25	Pro	HD1	T	2.30	2.90	−0.60	2.91	5.34
8	Lys	HG1	T	1.70	1.67	0.03	0.00	0.05	25	Pro	HD2	T	2.43	2.10	0.33	0.48	1.37
9	Asn	HN	B	8.67	8.73	−0.06	−0.14	0.04	26	Ala	HN	B	9.82	8.31	1.51	1.21	0.46
9	Asn	HA	B	4.53	4.62	−0.09	−0.12	0.03	26	Ala	HA	B	5.79	3.77	2.02	1.77	0.61
9	Asn	HB1	T	2.82	2.88	−0.06	−0.11	0.02	26	Ala	HB3	B	1.60	0.64	0.96	0.82	0.24
9	Asn	HB2	T	2.82	2.88	−0.06	−0.13	0.03	27	Tyr	HN	B	8.97	7.45	1.52	1.36	0.48
10	Lys	HN	B	8.48	8.88	−0.40	−0.25	0.07	27	Tyr	HA	B	4.45	4.06	0.39	0.58	0.39
10	Lys	HA	B	4.69	4.79	−0.10	−0.19	0.08	27	Tyr	HB1	S	2.96	2.67	0.29	0.19	0.22
10	Lys	HB1	S	2.07	2.20	−0.13	−0.23	0.18	27	Tyr	HB2	S	2.96	2.31	0.65	0.59	0.25
10	Lys	HB2	S	2.19	2.52	−0.33	−0.40	0.15	27	Tyr	HD1	T	6.48	5.76	0.72	0.57	0.33
10	Lys	HG1	T	1.68	1.76	−0.08	−0.21	0.10	27	Tyr	HD2	T	6.48	5.76	0.72	0.77	0.90
11	Gly	HN	B	7.57	7.82	−0.25	−0.31	0.09	27	Tyr	HE1	T	5.08	4.53	0.55	0.70	0.68
11	Gly	HA1	S	4.12	4.67	−0.55	−0.53	0.18	27	Tyr	HE2	T	5.08	4.53	0.55	2.12	4.33
11	Gly	HA2	S	3.69	3.96	−0.27	−0.39	0.13	28	Lys	HN	B	9.27	8.76	0.51	0.51	0.16
12	Cys	HN	T	7.85	8.45	−0.60	−0.65	0.27	28	Lys	HA	B	4.22	4.00	0.22	0.16	0.07
12	Cys	HA	T	2.95	4.92	−1.97	−1.88	1.50	28	Lys	HB1	T	2.05	1.76	0.29	0.26	0.07
12	Cys	HB1	S	2.49	2.99	−0.50	−0.62	1.73	28	Lys	HB2	T	1.95	1.54	0.41	0.18	0.05
12	Cys	HB2	S	2.95	3.27	−0.32	−0.32	0.58	28	Lys	HG1	T	1.55	1.22	0.33	0.32	0.09
13	Val	HN	B	6.76	6.58	0.18	−0.15	0.32	29	Asp	HN	B	7.14	6.73	0.41	0.41	0.15
13	Val	HA	B	4.35	3.58	0.77	0.60	0.45	29	Asp	HA	B	4.79	4.61	0.18	0.15	0.07
13	Val	HB	B	1.66	1.03	0.63	0.11	0.18	29	Asp	HB1	S	3.07	2.72	0.35	0.21	0.12
13	Val	HG13	S	0.80	0.85	−0.05	−0.06	0.12	29	Asp	HB2	S	3.07	2.58	0.49	0.43	0.19
13	Val	HG23	S	0.99	0.64	0.35	0.24	0.14	30	Val	HN	B	7.81	7.52	0.29	0.22	0.20
14	Ala	HN	B	6.94	7.36	−0.42	−0.31	0.36	30	Val	HA	B	3.92	4.12	−0.20	−0.24	0.17
14	Ala	HA	B	3.99	4.07	−0.08	−0.10	0.18	30	Val	HB	B	1.95	2.18	−0.23	−0.29	0.29
14	Ala	HB3	B	1.03	1.66	−0.63	−0.59	0.25	30	Val	HG13	S	0.50	1.52	−1.02	−1.00	0.41
15	Cys	HN	T	6.83	6.82	0.01	0.03	0.93	30	Val	HG23	S	0.54	0.68	−0.14	−0.13	0.62
15	Cys	HA	T	4.73	4.32	0.41	−0.08	0.60	31	Ala	HN	B	8.43	8.52	−0.09	−0.08	0.11
15	Cys	HB1	S	−0.27	0.94	−1.21	−2.05	2.62	31	Ala	HA	B	3.78	3.99	−0.21	−0.26	0.08
15	Cys	HB2	S	−0.07	1.82	−1.89	−2.80	3.81	31	Ala	HB3	B	1.50	1.57	−0.07	−0.10	0.06
16	His	HN	T	8.72	6.77	1.95	1.92	1.32	32	Ala	HN	B	7.62	7.55	0.07	−0.03	0.05
16	His	HA	T	7.75	3.64	4.11	4.23	1.97	32	Ala	HA	B	4.13	4.15	−0.02	−0.05	0.03
16	His	HB1	T	6.14	0.18	5.96	5.13	2.70	32	Ala	HB3	B	1.63	1.58	0.05	0.01	0.03
16	His	HB2	T	8.06	0.85	7.21	4.81	3.27	33	Lys	HN	B	7.65	7.78	−0.13	−0.10	0.05
17	Ala	HN	B	10.04	7.58	2.46	2.29	0.83	33	Lys	HA	B	4.01	4.05	−0.04	−0.10	0.03
17	Ala	HA	B	5.29	4.18	1.11	1.14	0.38	33	Lys	HB1	T	1.78	1.90	−0.12	−0.23	0.08
17	Ala	HB3	B	2.12	1.19	0.93	0.87	0.24	33	Lys	HB2	T	1.93	2.00	−0.07	−0.12	0.06
18	Ile	HN	B	8.93	8.16	0.77	0.71	0.20	34	Phe	HN	B	7.53	7.76	−0.23	−0.24	0.06
18	Ile	HA	B	4.04	3.13	0.91	0.89	0.27	34	Phe	HA	B	4.39	4.59	−0.20	−0.22	0.05
18	Ile	HB	B	2.07	1.57	0.50	0.44	0.14	34	Phe	HB1	T	2.42	2.73	−0.31	−0.32	0.07

Table I (Continued)

sequence	residue	atom	use	oxidized	reduced	obs	calc	gradient	sequence	residue	atom	use	oxidized	reduced	obs	calc	gradient
34	Phe	HB2	T	3.14	3.42	−0.28	−0.38	0.09	50	Asn	HA	B	5.57	4.47	1.10	1.06	0.29
34	Phe	HD1	T	7.28	7.63	−0.35	−0.56	0.17	50	Asn	HB1	T	3.43	2.58	0.85	0.74	0.19
34	Phe	HD2	T	7.28	7.63	−0.35	−0.27	0.06	50	Asn	HB2	T	3.43	2.58	0.85	0.80	0.22
34	Phe	HE1	T	7.20	7.63	−0.43	−0.68	0.22	51	Gly	HN	B	9.67	7.32	2.35	2.56	0.98
34	Phe	HE2	T	7.20	7.63	−0.43	−0.27	0.06	51	Gly	HA1	S	5.93	3.60	2.33	1.97	0.72
34	Phe	HZ1	T	7.20	7.64	−0.44	−0.42	0.12	51	Gly	HA2	S	6.60	2.00	4.60	3.98	1.78
35	Ala	HA	B	4.09	4.20	−0.11	−0.11	0.02	52	Ser	HN	B	9.67	7.12	2.55	2.70	1.50
35	Ala	HB3	B	1.47	1.53	−0.06	−0.10	0.02	52	Ser	HA	B	5.17	4.26	0.91	0.94	0.54
36	Gly	HN	B	8.60	8.71	−0.11	−0.11	0.02	52	Ser	HB1	T	3.85	2.80	1.05	1.54	2.14
36	Gly	HA1	T	3.80	3.88	−0.08	−0.10	0.01	52	Ser	HB2	T	4.03	2.80	1.23	1.60	1.44
36	Gly	HA2	T	4.02	4.06	−0.04	−0.13	0.02	53	Gln	HN	B	8.28	7.77	0.51	0.29	0.28
37	Gln	HN	B	7.73	7.81	−0.08	−0.15	0.03	53	Gln	HA	B	4.32	4.32	0.00	−0.08	0.28
37	Gln	HA	B	4.43	4.49	−0.06	−0.11	0.02	53	Gln	HB1	T	2.13	1.90	0.23	0.12	0.13
37	Gln	HB1	T	2.12	2.23	−0.11	−0.13	0.02	53	Gln	HB2	T	2.03	2.06	−0.03	0.20	0.21
37	Gln	HB2	T	2.27	2.38	−0.11	−0.17	0.03	53	Gln	HG1	X	2.30			−0.14	0.14
38	Ala	HN	B	8.67	8.78	−0.11	−0.10	0.01	54	Gly	HN	B	8.27	8.28	−0.01	−0.24	0.13
38	Ala	HA	B	4.18	4.26	−0.08	−0.10	0.02	54	Gly	HA1	S	4.09	4.19	−0.10	−0.09	0.06
38	Ala	HB3	B	1.37	1.44	−0.07	−0.08	0.01	54	Gly	HA2	S	3.75	3.89	−0.14	−0.14	0.05
39	Gly	HN	B	8.63	9.02	−0.39	−0.12	0.02	55	Val	HN	B	9.78	10.28	−0.50	−0.25	0.13
39	Gly	HA1	T	3.97	4.07	−0.10	−0.11	0.02	55	Val	HA	B	3.66	3.79	−0.13	−0.20	0.06
39	Gly	HA2	T	3.97	4.07	−0.10	−0.12	0.02	55	Val	HB	B	1.97	2.44	−0.47	−0.48	0.18
40	Ala	HN	B	7.48	7.63	−0.15	−0.18	0.03	55	Val	HG13	S	0.34	0.67	−0.33	−0.36	0.11
40	Ala	HA	B	3.88	4.06	−0.18	−0.25	0.05	55	Val	HG23	S	0.83	1.03	−0.20	−0.22	0.12
40	Ala	HB3	B	1.42	1.63	−0.21	−0.28	0.06	56	Trp	HN	B	10.08	10.65	−0.57	−0.40	0.13
41	Glu	HN	B	8.64	8.78	−0.14	−0.24	0.05	56	Trp	HA	B	4.52	4.63	−0.11	−0.19	0.09
41	Glu	HA	B	3.32	3.65	−0.33	−0.40	0.09	56	Trp	HB1	S	3.80	3.82	−0.02	−0.11	0.25
41	Glu	HB1	T	1.82	2.04	−0.22	−0.22	0.04	56	Trp	HB2	S	3.19	3.63	−0.44	−0.47	0.31
41	Glu	HB2	T	1.97	2.04	−0.07	−0.26	0.05	56	Trp	HD	B	6.82	7.72	−0.90	−0.95	0.41
42	Ala	HN	B	7.58	7.67	−0.09	−0.19	0.04	56	Trp	HNE	B	10.48	11.27	−0.79	−0.90	0.38
42	Ala	HA	B	3.98	4.11	−0.13	−0.16	0.04	56	Trp	HE	B	8.11	8.02	0.09	0.03	0.16
42	Ala	HB3	B	1.36	1.42	−0.06	−0.10	0.03	56	Trp	HZ1	B	7.24	7.59	−0.35	−0.40	0.19
43	Glu	HN	B	7.55	7.68	−0.13	−0.21	0.05	56	Trp	HZ2	B	7.38	7.27	0.11	0.06	0.11
43	Glu	HA	B	4.05	4.07	−0.02	−0.11	0.06	56	Trp	HH	B	7.12	7.12	0.00	−0.07	0.11
43	Glu	HB1	S	2.00	2.14	−0.14	−0.16	0.06	57	Gly	HN	B	7.68	7.93	−0.25	−0.25	0.07
43	Glu	HB2	S	1.74	1.94	−0.20	−0.22	0.06	57	Gly	HA1	S	4.39	4.58	−0.19	−0.24	0.09
44	Leu	HN	B	8.19	8.57	−0.38	−0.42	0.12	57	Gly	HA2	S	4.00	4.14	−0.14	−0.17	0.05
44	Leu	HA	B	3.22	3.89	−0.67	−0.74	0.30	58	Pro	HA	T	5.27	4.77	0.50	−0.18	0.05
44	Leu	HB1	S	0.17	1.36	−1.19	−1.29	0.45	58	Pro	HB1	T	2.58	2.25	0.33	−0.14	0.03
44	Leu	HB2	S	1.23	1.93	−0.70	−0.75	0.22	58	Pro	HB2	T	2.23	2.25	−0.02	−0.17	0.04
44	Leu	HG	T	0.79	1.73	−0.94	−0.72	0.21	58	Pro	HG1	T	1.75	2.29	−0.54	−0.16	0.03
44	Leu	HD13	S	−0.14	0.80	−0.94	−1.06	0.33	58	Pro	HG2	T	1.57	2.05	−0.48	−0.28	0.05
44	Leu	HD23	S	−0.33	0.85	−1.18	−1.30	0.48	58	Pro	HD1	T	2.85	3.70	−0.85	−0.23	0.06
45	Ala	HN	B	7.99	8.27	−0.28	−0.39	0.13	58	Pro	HD2	T	2.98	3.93	−0.95	−0.16	0.04
45	Ala	HA	B	3.49	3.82	−0.33	−0.42	0.20	59	Ile	HN	B	7.01	7.39	−0.38	−0.42	0.12
45	Ala	HB3	B	1.24	1.36	−0.12	−0.20	0.08	59	Ile	HA	B	4.18	4.66	−0.48	−0.40	0.13
46	Gln	HN	B	7.44	7.37	0.07	−0.05	0.09	59	Ile	HB	B	1.34	2.16	−0.82	−0.68	0.21
46	Gln	HA	B	4.18	3.82	0.36	0.28	0.11	59	Ile	HG11	T	0.60	1.82	−1.22	−1.11	0.41
46	Gln	HB1	T	2.34	2.11	0.23	0.13	0.09	59	Ile	HG12	T	0.95	1.50	−0.55	−0.63	0.21
46	Gln	HB2	T	2.59	2.38	0.21	0.10	0.06	59	Ile	HG23	T	0.20	1.32	−1.12	−0.39	0.10
47	Arg	HN	B	7.84	7.62	0.22	0.12	0.21	60	Pro	HA	T	4.48	4.86	−0.38	−0.20	0.40
47	Arg	HA	B	4.83	3.70	1.13	1.05	0.47	61	Met	HN	T	9.15	8.65	0.50	0.44	1.34
47	Arg	HB1	S	1.60	0.83	0.77	0.73	0.78	61	Met	HA	T	1.24	3.63	−2.39	−1.79	2.96
47	Arg	HB2	S	1.60	1.72	−0.12	−0.14	0.52	61	Met	HB1	S	6.19	−0.91	7.10	7.29	6.55
47	Arg	HG1	S	1.80	1.78	0.02	0.05	0.19	61	Met	HB2	S	−1.67	−2.75	1.08	2.89	13.87
47	Arg	HG2	S	1.95	1.75	0.20	0.36	0.25	61	Met	HG1	T	−9.30	−0.52	−8.78	9.11	15.07
47	Arg	HD1	T	3.36	3.05	0.31	0.02	0.25	61	Met	HG2	T	−33.70	−3.56	−30.14	13.82	9.94
47	Arg	HD2	T	3.27	3.15	0.12	−0.36	0.32	61	Met	HE3	T	−14.87	−2.96	−11.91	9.55	13.23
47	Arg	HE	T	7.55	7.27	0.28	−0.06	0.11	63	Pro	HA	T	5.54	3.23	2.31	2.25	0.83
48	Ile	HN	B	8.35	8.06	0.29	0.21	0.52	63	Pro	HB1	T	3.17	2.05	1.12	1.13	0.32
48	Ile	HA	B	4.66	1.47	3.19	3.44	2.97	63	Pro	HB2	T	2.43	1.52	0.91	0.93	0.27
48	Ile	HB	B	1.67	1.62	0.05	−0.15	0.50	63	Pro	HG1	T	2.55	1.75	0.80	0.70	0.18
48	Ile	HG11	S	−0.48	1.01	−1.49	−1.70	1.10	63	Pro	HG2	T	2.55	1.63	0.92	0.68	0.20
48	Ile	HG12	S	−2.49	1.76	−4.25	−4.11	3.02	73	Pro	HD1	T	4.00	3.28	0.72	0.75	0.26
48	Ile	HG23	T	0.82	0.62	0.20	−0.34	1.10	63	Pro	HD2	T	4.30	3.22	1.08	1.00	0.32
48	Ile	HD3	T	0.08	1.32	−1.24	−1.94	0.86	64	Asn	HN	B	9.02	6.89	2.13	1.95	0.78
49	Lys	HN	B	8.07	7.06	1.01	0.87	0.42	64	Asn	HA	B	5.90	4.80	1.10	1.02	0.58
49	Lys	HA	B	4.94	3.83	1.11	1.15	0.47	64	Asn	HB1	S	3.06	2.05	1.01	0.85	0.65
49	Lys	HB1	T	2.23	1.58	0.65	0.60	0.20	64	Asn	HB2	S	4.03	2.43	1.60	1.74	0.97
49	Lys	HB2	T	1.90	1.33	0.57	0.48	0.20	65	Ala	HN	B	9.05	8.63	0.42	0.40	0.26
49	Lys	HG1	T	1.80	1.20	0.60	0.53	0.17	65	Ala	HA	B	4.91	4.50	0.41	0.33	0.13
49	Lys	HG2	T	1.41	1.20	0.21	0.62	0.17	65	Ala	HB3	B	1.52	1.32	0.20	0.14	0.10
49	Lys	HD	X	3.27			0.34	0.09	66	Val	HN	B	8.05	7.62	0.43	0.42	0.19
50	Asn	HN	B	9.32	7.98	1.34	1.22	0.41	66	Val	HA	B	5.00	4.83	0.17	0.10	0.09

Table I (Continued)

sequence	residue	atom	use	oxidized	reduced	obs	calc	gradient	sequence	residue	atom	use	oxidized	reduced	obs	calc	gradient
66	Val	HB	B	2.53	2.44	0.09	0.07	0.13	77	Trp	HD	B	7.12	7.25	−0.13	−0.13	0.04
66	Val	HG13	S	0.87	0.74	0.13	0.01	0.21	77	Trp	HNE	B	10.08	10.03	0.05	−0.05	0.04
66	Val	HG23	S	1.03	0.63	0.40	0.41	0.28	77	Trp	HE	B	6.80	7.34	−0.54	−0.52	0.20
67	Ser	HN	B	9.12	9.06	0.06	0.06	0.06	77	Trp	HZ1	B	7.23	7.05	0.18	0.05	0.07
67	Ser	HA	B	4.71	4.57	0.14	0.13	0.05	77	Trp	HZ2	B	6.06	6.37	−0.31	−0.24	0.29
67	Ser	HB1	T	4.45	4.40	0.05	0.05	0.03	77	Trp	HH	B	6.32	5.78	0.54	0.14	0.17
67	Ser	HB2	T	4.00	3.93	0.07	0.06	0.03	78	Val	HN	B	8.28	9.09	−0.81	−0.64	0.19
68	Asp	HN	B	8.93	8.82	0.11	0.09	0.04	78	Val	HA	B	2.45	2.57	−0.12	−0.37	0.17
68	Asp	HA	B	4.38	4.27	0.11	0.08	0.05	78	Val	HB	B	1.33	2.21	−0.88	−1.08	0.37
68	Asp	HB1	T	2.71	2.62	0.09	0.03	0.02	78	Val	HG13	S	−0.10	0.48	0.58	−0.91	0.41
68	Asp	HB2	T	2.71	2.62	0.09	0.07	0.03	78	Val	HG23	S	−0.63	0.63	−1.26	−1.32	0.62
69	Asp	HN	B	8.38	8.36	0.02	0.00	0.03	79	Leu	HN	B	7.28	7.64	−0.36	−0.51	0.14
69	Asp	HA	B	4.37	4.38	−0.01	−0.07	0.03	79	Leu	HA	B	3.59	3.83	−0.24	−0.33	0.09
69	Asp	HB1	T	2.58	2.60	−0.02	−0.03	0.02	79	Leu	HB1	T	1.59	1.92	−0.33	−0.28	0.06
69	Asp	HB2	T	2.58	2.60	−0.02	−0.06	0.02	79	Leu	HB2	T	1.41	1.58	−0.17	−0.34	0.08
70	Glu	HN	B	7.78	7.76	0.02	−0.04	0.04	79	Leu	HG	B	1.30	1.85	−0.55	−0.57	0.15
70	Glu	HA	B	3.76	3.83	−0.07	−0.15	0.05	79	Leu	HD13	T	0.52	0.85	−0.33	−0.39	0.09
70	Glu	HB1	T	2.47	2.48	−0.01	−0.13	0.07	79	Leu	HD23	T	0.56	0.93	−0.37	−0.42	0.10
70	Glu	HB2	T	1.58	1.67	−0.10	−0.04	0.06	80	Ser	HN	B	7.22	7.44	−0.22	−0.25	0.06
70	Glu	HG1	T	2.26	2.35	−0.09	−0.05	0.03	80	Ser	HA	B	4.33	4.43	−0.10	−0.13	0.03
71	Ala	HN	B	8.77	8.72	0.05	−0.06	0.08	80	Ser	HB1	B	3.83	4.00	−0.17	−0.16	0.03
71	Ala	HA	B	3.68	3.92	−0.24	−0.31	0.18	80	Ser	HB2	T	3.83	4.00	−0.17	−0.10	0.02
71	Ala	HB3	B	1.62	1.62	0.00	0.00	0.13	81	Gln	HN	B	7.06	7.12	−0.06	−0.13	0.05
72	Gln	HN	B	7.98	8.08	−0.10	−0.16	0.06	81	Gln	HA	B	3.95	3.89	0.06	0.01	0.03
72	Gln	HA	B	3.72	3.96	−0.24	−0.28	0.08	81	Gln	HB1	T	1.63	1.52	0.11	0.11	0.06
72	Gln	HB1	T	2.11	2.22	−0.11	−0.18	0.04	81	Gln	HB2	T	1.63	1.72	−0.09	0.02	0.07
72	Gln	HB2	T	2.26	2.22	0.04	−0.15	0.04	82	Lys	HN	B	7.36	7.43	−0.07	−0.06	0.03
72	Gln	HG1	T	2.42	2.36	0.06	−0.10	0.03	82	Lys	HA	B	4.07	4.05	0.02	0.01	0.02
73	Thr	HN	B	7.99	8.15	−0.16	−0.23	0.06	82	Lys	HB1	T	1.65	1.61	0.04	−0.07	0.02
73	Thr	HA	B	3.70	3.91	−0.21	−0.25	0.05	82	Lys	HB2	T	1.70	1.70	0.00	−0.04	0.03
73	Thr	HB	B	4.10	4.28	−0.18	−0.24	0.06	82	Lys	HG1	T	1.29	1.28	0.01	−0.02	0.02
73	Thr	HG3	B	1.02	1.23	−0.21	−0.21	0.04	5		HHC1	H	9.15	9.85	−0.70	−4.20	3.45
74	Leu	HN	B	8.12	8.56	−0.44	−0.44	0.12	10		HHD1	H	0.20	9.34	−9.14	−10.63	7.18
74	Leu	HA	B	3.66	4.30	−0.64	−0.61	0.17	15		HHA1	H	6.40	9.24	−2.84	−4.62	3.25
74	Leu	HB1	S	0.40	1.72	−1.32	−1.27	0.47	20		HHB1	H	−1.20	9.22	−10.42	−10.71	7.23
74	Leu	HB2	S	1.57	2.32	−0.75	−0.78	0.28	2	1	HMB3	H	24.30	3.67	20.63	−3.13	1.70
74	Leu	HG	T	1.42	1.80	−0.38	−0.50	0.15	7	1	HMC3	H	14.10	3.74	10.36	−2.98	1.64
74	Leu	HD13	T	0.31	1.20	−0.89	−0.66	0.28	12	1	HMD3	H	29.00	3.30	25.70	−3.12	1.71
74	Leu	HD23	T	0.58	1.24	−0.66	−0.68	0.23	18	1	HMA3	H	15.70	3.39	12.31	−4.48	2.30
75	Ala	HN	B	8.03	8.76	−0.73	−0.68	0.20	3	1	HAB1	H	4.10	5.96	−1.86	−1.63	1.22
75	Ala	HA	B	2.86	3.92	−1.06	−1.16	0.37	3	2	HBB3	H	2.65	1.84	0.81	−0.48	0.92
75	Ala	HB3	B	1.04	1.56	−0.52	−0.66	0.19	8	1	HAC1	H	−0.14	6.15	−6.29	−5.55	2.94
76	Lys	HN	B	7.84	8.11	−0.27	−0.46	0.11	8	2	HBC3	H	0.28	2.40	−2.12	−2.78	1.26
76	Lys	HA	B	3.59	3.88	−0.29	−0.35	0.07	13	1A	HAD1	H	12.60	4.26	8.34	−1.61	0.85
76	Lys	HB1	T	1.74	1.96	−0.22	−0.30	0.06	13	1B	HAD2	H	11.20	4.57	6.63	−1.74	1.08
76	Lys	HB2	T	1.42	1.45	−0.03	−0.27	0.05	13	2A	HBD1	H	0.20	2.67	−2.47	−1.10	1.40
76	Lys	HG	X	1.27			−0.20	0.04	13	2B	HBD2	H	1.70	3.43	−1.73	−1.03	0.94
77	Trp	HN	B	7.56	7.85	−0.29	−0.43	0.10	17	1A	HAA1	H	5.70	4.68	1.02	−2.92	1.72
77	Trp	HA	B	4.11	4.35	−0.24	−0.25	0.06	17	1B	HAA2	H	1.00	3.90	−2.90	−3.02	1.52
77	Trp	HB1	S	3.13	3.55	−0.42	−0.42	0.12	13	2A	HBA1	H	0.55	3.35	−2.80	−2.63	1.50
77	Trp	HB2	S	3.02	3.21	−0.19	−0.27	0.07	13	2B	HBA2	H	0.33	2.72	−2.39	−2.44	1.80

[a] Chemical shifts in ppm are for 323 K and pH 5.2. The sequence and residue columns give the residue number and type except for heme protons. In this case, column 1 gives the standard IUB-IUPAC label for the tetrapyrrole position and column 2 gives the superscript label for extended labels along the substituent, as depicted in Figure 1 of Chau et al. (1990). The atom column gives the name of the proton according to the conventions of the Brookhaven Protein Data Bank. The use column gives a code label designating the following: B, the proton was used in the basis set for the optimization of the NMR effective anisotropy; S, stereospecifically assigned proton as discussed in the text; T, not reliably stereospecifically assigned, but used in the test for structural change as described in the text; X, a proton assigned in the oxidized, but not in the reduced state; H, a heme proton. The oxidized and reduced columns give the oxidized and reduced chemical shifts, respectively. The obs column is $\delta_{pc,obs}$ and calc is $\delta_{pc,calc}$, as defined in the text. The gradient column is the gradient computed by eq 3.

ment. The final specific sites of detected structural differences were in very good agreement in spite of the alternative screens [see Table III of Feng et al. (1990) and Table IV of Gao et al. (1991)].

Since there is limited effective resolution, there can be structural changes not detected by examination of $\delta_{pc,obs}$. In a previous study (Cai et al., 1992) on reduced *c*-551 from *P. aeruginosa* and *P. stutzeri*, a loop region from residues 34–40 was found to be very mobile in solution, while the crystal structure for reduced *c*-551 captured only one conformer. This region is relatively far from the iron; the critical residues 36–38 are on the order of 20 Å away. The values of $\delta_{pc,obs}$ and $\delta_{pc,calc}$ generally agree, but they are on the order of 0.1 ppm, which is the same as $\langle\delta_{pc}\rangle$, so that it would be difficult to detect any discrepancy.

The present study on *P. aeruginosa c*-551 indicates that the structures of reduced and oxidized forms of *c*-551 are sufficiently similar that NMR observations of $\delta_{ox} - \delta_{red}$ in connection with pseudocontact shift calculations may become a new class of NMR constraints for solution structure determinations of cytochromes from other species, for which no crystallographic study has been accomplished. The paramagnetic effects are very strong for protons close to the iron. The magnitude of the gradient of the pseudocontact scalar field was 13.9 Å/ppm for Met 61 β-protons and 6.1 Å/ppm for a Gly 24 proton. The effect falls off rapidly with

distance r from the iron, but even at 11 Å gradients of 0.25 Å/ppm are possible. As the distance increases, the magnitude of the effect falls off, but the number of resonances that are within the expanding volume increases. In practice, it may be necessary to construct a penalty function for any pseudocontact constraint, as has been done traditionally for NMR constraints based upon coupling constants or NOE enhancements, to cover uncertainties in the measurements and in the assumption of no redox-related structural change. Many practical implementation details remain to be solved, but the potential for a new class of NMR-based constraints seems high.

REFERENCES

Baker, B. R., Basolo, F., & Neuman, H. M. (1959) *J. Phys. Chem. 63*, 371–381.

Bartocci, C., Scandola, F., Ferri, A., & Carassiti, V. (1980) *J. Am. Chem. Soc. 102*, 7067–7072.

Cai, M., & Timkovich, R. (1991) *Biochem. Biophys. Res. Commun. 178*, 309–314.

Cai, M., Bradford, E. G., & Timkovich, R. (1992) *Biochemistry 31*, 8603–8612.

Chao, Y.-Y. H., Bersohn, R., & Aisen, P. (1979) *Biochemistry 18*, 774–779.

Chau, M. H., Cai, M., & Timkovich, R. (1990) *Biochemistry 29*, 5076–5087.

Del Gaudio, J., & La Mar, G. N. (1978) *J. Am. Chem. Soc. 100*, 1112–1119.

Detlefsen, D. J., Thanabal, V., Pecoraro, V. L., & Wagner, G. (1990) *Biochemistry 29*, 9377–9386.

Emerson, S. D., & La Mar, G. N. (1990) *Biochemistry 29*, 1556–1566.

Feng, Y., Roder, H., Englander, S. W., Wand, A. J., & DiStefano, D. L. (1989) *Biochemistry 28*, 195–203.

Feng, Y., Roder, H., & Englander, S. W. (1990) *Biochemistry 29*, 3494–3504.

Gadsby, P. M. A., & Thomson, A. J. (1990) *J. Am. Chem. Soc. 112*, 5003–5001.

Gao, Y., Boyd, J., Pielak, G. J., & Williams, R. J. P. (1991) *Biochemistry 30*, 1928–1934.

Horrocks, W. D., Jr., & Greenberg, E. S. (1973) *Biochim. Biophys. Acta 322*, 38–44.

Keller, R. M., & Wuthrich, K. (1976) *FEBS Lett. 70*, 180–183.

Keller, R. M., & Wuthrich, K. (1978) *Biochem. Biophys. Res. Commun. 83*, 1132–1139.

Kuszewski, J., Nilges, M., & Brunger, A. T. (1992) *J. Biomol. NMR 2*, 33–56.

Leitch, F. A., Moore, G. R., & Pettigrew, G. W. (1984) *Biochemistry 23*, 1831–1838.

Mandel, N., Mandel, G., Truss, B. L., Rosenberg, J., Carlson, G., & Dickerson, R. E. (1977) *J. Biol. Chem. 252*, 4619–4636.

Matsuura, Y., Takano, T., & Dickerson, R. E. (1982) *J. Mol. Biol. 156*, 389–409.

Rajarathnam, K., La Mar, G. N., Chiu, M. L., & Sligar, S. G. (1992) *J. Am. Chem. Soc. 114*, 9048–9058.

Rajarathanam, K., Qin, J., La Mar, G. N., Chiu, M. L., & Sligar, S. G. (1993) *Biochemistry 32*, 5670–5680.

Senn, H., Keller, R. M., & Wuthrich, K. (1980) *Biochem. Biophys. Res. Commun. 92*, 1362–1369.

Swanson, R., Trus, B. L., Mandel, N., Mandel, G.. Kallai, O. B., & Dickerson, R. E. (1977) *J. Biol. Chem. 252*, 759–775.

Takano, T., & Dickerson, R. E. (1982a) *J. Mol. Biol. 153*, 79–94.

Takano, T., & Dickerson, R. E. (1982b) *J. Mol. Biol. 153*, 95–116.

Takano, T., Kallai, O. B., Swanson, R., & Dickerson, R. E. (1973) *J. Biol. Chem. 248*, 5234–5255.

Takano, T., Trus, B. L., Mandel, N. Mandel, G., Kallai, O. B., Swanson, R., & Dickerson, R. E. (1977) *J. Biol. Chem. 252*, 776–785.

Timkovich, R. (1991) *Inorg. Chem. 30*, 37–42.

Timkovich, R., Cai, M., & Dixon, D. W. (1988) *Biochem. Biophys. Res. Commun. 150*, 1044–1050.

Turner, D. L., & Williams, R. J. P. (1993) *Eur. J. Biochem. 211*, 555–562.

Veitch, N. C., Whitford, D., & Williams, R. J. P. (1990) *FEBS Lett. 269*, 297–304.

Williams, G., Clayden, N. J., Moore, G. R., & Williams, R. J. P. (1985) *J. Mol. Biol. 183*, 447–460.

Yu, C., Chiang, Y.-L., Yu, L., & King, T. E. (1975) *J. Biol. Chem. 250*, 6218–6221.